An Integrated Observer Framework Based Mechanical Parameters Identification for Adaptive Control of Permanent Magnet Synchronous Motor

Zhong Liao, Zhaohua Liu*, Lei Chen, Mingyang Lyu, Dian Wang, Faming Wu, Zhengheng Wang, and Hualiang Wei

Abstract: An integrated observer framework based mechanical parameters identification approach for adaptive control of permanent magnet synchronous motors is proposed in this paper. Firstly, an integrated observer framework is established for mechanical parameters' estimation, which consists of an extended sliding mode observer (ESMO) and a Luenberger observer. Aiming at minimizing the influence of parameters coupling, the viscous friction and the moment of inertia are obtained by ESMO and the load torque is identified by Luenberger observer separately. After obtaining estimates of the mechanical parameters, the optimal proportional integral (PI) parameters of the speed-loop are determined according to third-order best design method. As a result, the controller can adjust the PI parameters in real time according to the parameter changes to realize the adaptive control of the system. Meanwhile, the disturbance is compensated according to the estimates. Finally, the experiments were carried out on simulation platform, and the experimental results validated the reliability of parameter identification and the efficiency of the adaptive control strategy presented in this paper.

Key words: parameter identification; permanent magnet synchronous motor; adaptive control; extended sliding mode observer; Luenberger observer

1 Introduction

The permanent magnet synchronous motor (PMSM) is

- Zhong Liao, Zhaohua Liu, Lei Chen, Mingyang Lyu, and Zhengheng Wang are with the School of Information and Electrical Engineering, Hunan University of Science and Technology, Xiangtan 411201, China. E-mail: zhongliao@ mail.hnust.edu.cn; zhaohualiu2009@hotmail.com; chenlei@ hnust.edu.cn; 1040133@hnust.edu.cn; dukehenry83@outlook. com.
- Dian Wang and Faming Wu are with the Wind Power Business Division, CRRC Zhuzhou Institute Co., Ltd., Zhuzhou 412001, China. E-mail: wangdian@csrzic.com; wufm@csrzic.com.
- Hualiang Wei is with the Department of Automatic Control and Systems Engineering, University of Sheffield, Sheffield, S1 3JD, UK. E-mail: w.hualiang@sheffield.ac.uk.
- * To whom correspondence should be addressed.
  Manuscript received: 2022-05-27; revised: 2022-08-08; accepted: 2022-10-18

becoming increasingly used in aerospace, national defense, electric vehicle drive, robotics, and other sectors due to its advantages of compact size, simple construction, high power density, strong stability, high power factor, stable and reliable operation, etc.[1−4] The precision and dependability of motor control systems are becoming increasingly important in numerous sectors with the development of scientific, technical, and social level. The PMSM has good control performance when using the traditional vector proportional integral (PI) control method, but the parameters of the motor may change when the motor is operating under long time running, temperatures variation, loads change, or other variable application scenarios, which will give rise to the deterioration of controller's performance[5]. Therefore, precise identification of the system's mechanical parameters allows the controller gains to be modified immediately

according to the identification results, thereby improving control performance and increasing system robustness[6].

Some researchers have investigated a number of parameter identification approaches to address the problem of suboptimal controller impact and poor robustness caused by PMSM parameter changes. Model reference adaptation system (MRAS) and recursive least squares (RLS) are the most extensively utilized identifying approaches. Additionally, approaches such as the extended Kalman filter (EKF), observer method, and artificial intelligence method also have been used to identify PMSM parameters.

The MRAS method offers the benefits of simple design, unambiguous physical meaning, and high identification accuracy[7], whose core content is the design of the adaptive law. The most prevalent adaptive law design approaches are the MIT rule, Lyapunov stability theory, and Popov hyperstability theory. MIT rule method is simple, but it ignores the issue of stability[8]. Lyapunov method considers the system stability problem[9], but the construction of Lyapunov function is difficult. On the contrary, the Popov hyperstability theorem, which not only considers system stability but also has a simpler design, is commonly utilized in parameter identification. In Ref. [10], Popov's criterion based MRAS adaptive strategy has been used for speed estimation.

RLS method has become a very widespread parameter estimation algorithm today, particularly RLS with forgetting factors, which is frequently employed to overcome the problems of asymptotic parameters and data saturation[11−14]. EKF method is a relatively optimal state parameter estimation method, which has good identification results in practical applications, but it requires additional computations, including the inverse calculation of high-order matrices[15−18]. Besides, both RLS and EKF take longer to perform parameter estimation and their convergence depends on the initial state of the system.

Artificial intelligence methods mainly include fuzzy control methods, neural networks, particle swarm algorithms, genetic algorithms[19−21], etc. In Ref. [22], a parameter identification method combining fuzzy functions with MRAS is proposed. Considering the deficiency of the parameter identification algorithm of PMSM, Ref. [23] proposed a method merging Elman neural network with modified EKF to identify multiple parameters. Artificial intelligence methods have high recognition accuracy and speed under certain conditions, but they necessitate a great deal of computation and are therefore more demanding for the processor and user.

The observer method is divided into two main types: disturbance observers (DOB) and sliding mode observers (SMO). The DOB detects disturbances rapidly and allows the system to respond to variable loads more quickly[24]. The SMO has the advantages of poor parameter sensitivity and strong system robustness[25, 26]. In Ref. [27], an improved SMO was proposed to realize high precision identification of load torque under different speed ranges. However, traditional low-order SMO has problems such as chattering and slow response which requires additional filters in the system to obtain more accurate identification results[28], which may lead to delays and amplitude degradation of the identification results. When using the SMO for multi-parameter identification, there is a coupling effect between the parameters according to the motor equation of motion, as a result, inaccurate identification of one parameter affects the other parameters directly.

After obtaining the needed mechanical parameter values, they are commonly applied to the control system to enable the system to adapt or compensate the controller gains in response to external parameter changes[29, 30], so as to improve the anti-interference ability and response speed of the system. However, the effect of the viscous coefficient is ignored in most papers about adaptive control[31].

This paper presents a method for mechanical parameters identification based on an integrated observer framework. The error values of the mechanical parameters are utilized to establish an extended state equation that will be used to develop an extended sliding mode observer (ESMO). A simple algorithm for the identification of mechanical parameters is designed based on this observer, whose structure is comparable to a filter and thus avoids the effect of using additional filters. After the values of the friction coefficient and the moment of inertia are obtained by the ESMO, the load torque can be calculated directly according to the equations of motion, but in order to decrease the impact of coupling between the parameters and ensure the reliability of the parameter identification results, a separate identification of the load torque is carried out by Luenberger observer. Finally, the control system is calibrated based on the third-order best design method according to the obtained parameter values, and an

optimal algorithm for parameter self-tuning and compensation of disturbances is designed.

Simulation experiments have been carried out on MATLAB/Simulink platform to validate the accuracy of the mechanical parameter identification and the effectiveness of the self-tuning and compensation system.

The contributions of this paper are as follows:

(1) An ESMO is proposed to achieve the identification of the viscous friction coefficient and the moment of inertia, whose equivalent low pass filter (LPF) may avoid the chattering, phase lag, and amplitude decay generated by the usage of additional filter, and the identification results possess poor parameter sensitivity and high accuracy.

(2) A separate identification of the load torque is carried out by the Luenberger observer, which is helpful for achieving parameter decoupling and high-precision identification.

(3) The identified three mechanical parameter values are used in the adaptive control of the system to make it have better control performance.

The rest of this paper is organized as follows. Section 2 discusses the mechanical parameters identification methods. Section 3 introduces the adaptive gains adjustment and disturbance compensation method. Section 4 shows the simulation verification. Finally, Section 5 brings the conclusion of this paper.

2　Mechanical Parameters Identification

Due to the strong coupling and complexity of the control system of PMSM, an accurate mathematical model must be established to guarantee the control effect, neglecting the impact of magnetic field saturation, iron losses, eddy current losses, and other

factors. In the rotating d-q coordinate system, the mathematical model of PMSM can be expressed as

$$u_d = R_s i_d + L_d \frac{\mathrm{d}i_d}{\mathrm{d}t} - \omega_e L_q i_q \tag{1}$$

$$u_q = R_s i_q + L_d \frac{\mathrm{d}i_q}{\mathrm{d}t} + \omega_e (L_d i_d + \psi) \tag{2}$$

$$T_e = \frac{3}{2} P \left[\psi i_q + \left(L_d - L_q \right) i_d i_q \right] \tag{3}$$

$$T_e - T_L = J\dot{\omega} + B\omega \tag{4}$$

where u_d and u_q denote the stator voltages of d-q axis; i_d and i_q denote the stator currents of d-q axis; L_d and L_q denote the inductances of d-q axis; and R_s, P, ω_e, ω, J, B, T_e, T_L, and ψ denote the stator resistance, number of pole pairs, electrical angular velocities, mechanical angular velocities, moment of inertia, viscous friction coefficient, electromagnetic torque, load torque, and flux linkage, respectively. Equations (1) and (2) are the electrical model of the PMSM. Equation (3) is the electromagnetic torque equation of the PMSM, and since the cross-axis has the same inductance as the straight-axis, its electromagnetic torque equation is simplified to $T_e = 1.5P\psi i_q$. And Eq. (4) is the equation of motion. In Eqs. (1) and (2), R_s, L_d, L_q, and ψ are the electrical parameters. In Eq. (4), B, J, and T_L are the mechanical parameters. Generally, the speed loop is influenced by the mechanical parameters but the mechanical parameters cannot be measured directly. Considering the coupling between the mechanical parameters, the load torque is identified separately.

The framework of mechanical parameter identification under typical vector control is shown in Fig. 1. Figure 2 shows the integrated observer framework.
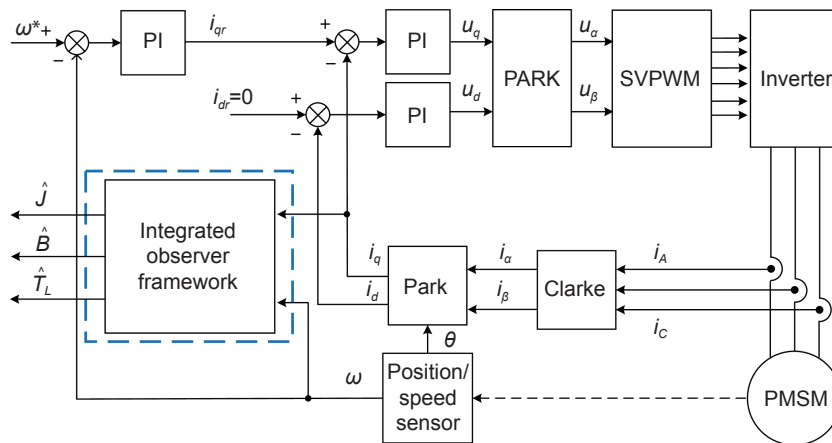

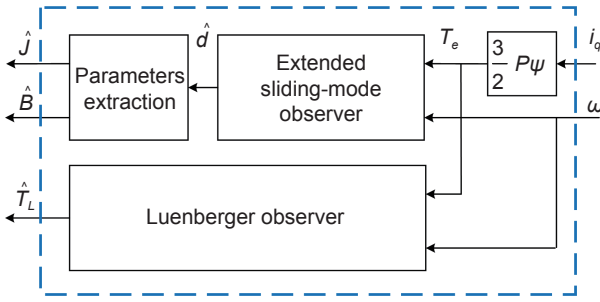Fig. 1　Framework of mechanical parameter identification.

Fig. 2   Integrated observer framework.

2.1   ESMO-based viscous friction coefficient and moment of inertia identification

Taking the effect of system disturbances into account, the dynamics equations of the motor are as follows:

$$J_0 \dot{\omega} = T_e - B_0 \omega + d \tag{5}$$

where $J = J_0 + \Delta J$, $B = B_0 + \Delta B$, and J_0 and B_0 are the rough estimates of the actual values of motor's J and B, respectively, which can usually be obtained empirically; ΔJ and ΔB denote the parameter errors between the actual value and rough estimates, respectively; and d represents the disturbance, which consists of motor parameter errors and external load condition, expressed as

$$d = -\Delta J \dot{\omega} - \Delta B \omega - T_L \tag{6}$$

At this point, the extended state equations are established as stated in Eq. (7),

$$\begin{cases} J_0 \dot{\omega} = T_e - B_0 \omega + d, \\ \dot{d} = -\Delta J \ddot{\omega} - \Delta B \dot{\omega} - \dot{T}_L = r \end{cases} \tag{7}$$

where d is selected as the extended system state and r denotes the derivative of d.

To obtain the motor mechanical parameters, the ESMO is designed as

$$\begin{cases} J_0 \dot{\hat{\omega}} = T_e - B_0 \hat{\omega} + \hat{d} + u_{smo}, \\ \dot{\hat{d}} = n u_{smo} \end{cases} \tag{8}$$

where $\hat{d}$, $\hat{\omega}$, n, and u_{smo} denote the estimated value of the disturbance, the estimated value of mechanical angular velocities, the sliding mode parameter, and the sliding mode observer signal, respectively, and u_{smo} is expressed as

$$u_{smo} = \eta \cdot \text{sgn}(S) \tag{9}$$

where η denotes the sliding mode gain and S denotes the sliding mode surface, that can be stated to be $S = \hat{\omega} - \omega$.

The following error equation can be derived from Eqs. (7) and (8):

$$\begin{cases} J_0 \dot{e}_1 = -B_0 e_1 + e_2 + u_{smo}, \\ \dot{e}_2 = n u_{smo} - r \end{cases} \tag{10}$$

where $e_1 = \hat{\omega} - \omega$ and $e_2 = \hat{d} - d$.

To ensure that the sliding mode can be achieved, the observer parameters are chosen according to the Lyapunov function $V = 0.5 s^2$. The derivation leads to the following relation:

$$\dot{V} = s \cdot \dot{s} = e_1 \cdot \dot{e}_1 \tag{11}$$

According to Eqs. (10) and (11), it can be obtained that

$$\dot{V} = \frac{1}{J_0} e_1 (-B_0 e_1 + e_2 + u_{smo}) =$$
$$\frac{1}{J_0} e_1 \left[(e_2 - B_0 e_1) + \eta \cdot \text{sgn}(e_1) \right] =$$
$$\begin{cases} \frac{1}{J_0} e_1 \left[(e_2 - B_0 e_1) + \eta \right], & e_1 > 0; \\ \frac{1}{J_0} e_1 \left[(e_2 - B_0 e_1) - \eta \right], & e_1 < 0 \end{cases} \tag{12}$$

The Lyapunov function's stability requirement condition requires: $\dot{V} = s \cdot \dot{s} = e_1 \cdot \dot{e}_1 < 0$, that is

$$\dot{V} = \begin{cases} \frac{1}{J_0} e_1 \left[(e_2 - B_0 e_1) + \eta \right], & e_1 > 0; \\ \frac{1}{J_0} e_1 \left[(e_2 - B_0 e_1) - \eta \right], & e_1 < 0 \end{cases} \tag{13}$$

It can therefore be obtained that

$$\eta < -|e_2 - B_0 e_1| \tag{14}$$

Equation (13) and Formula (14) show that the stability of the system is satisfied when η is negative.

The above analysis of the stability conditions for the Lyapunov function leads to the conclusion that e_1 and $\dot{e}_1$ also will converge to zero when the sliding mode occurs, that is, $e_1 = \dot{e}_1 = 0$, rewriting Eq. (10) as

$$\begin{cases} e_2 = -u_{smo}, \\ \dot{e}_2 = n u_{smo} - r \end{cases} \tag{15}$$

$$\dot{e}_2 + n e_2 + r = 0 \tag{16}$$

Calculating Eq. (16) gives the value of e_2 as

$$e_2 = e^{-nt} \left[C + \int r \cdot e^{nt} dt \right] \tag{17}$$

where C is a constant. In order to make sure e_2 can converge to zero, the following condition needs to be met

$$n > 0 \tag{18}$$

Meanwhile, in order to ensure reliable convergence of e_2, it is necessary to ensure that the value of n is large enough on the basis of $n > 0$, where the length of convergence time depends on the value of n as well.

It is obvious that the selection of the parameters of ESMO is governed by Formulas (14) and (18). Following the foregoing analysis, a structural block

diagram is generated as illustrated in Fig. 3.

When the sliding mode occurs, the velocity can be expressed as $w = \hat{w}$. Combining Eqs. (7) and (8), we can get

$$\dot{\hat{d}} + n\hat{d} = nd \quad \left(\hat{d} = \frac{n}{s+n} \cdot d \right) \tag{19}$$

It is clear that Eq. (19) is equivalent to a low-pass filter's transfer function whose cut-off frequency is specified by n. Therefore, the output of this observer will not include the chattering signals generated by additional filters.

As a result, the mechanical parameters contained in the disturbance estimates can be extracted. The structural block diagram of the ESMO is built as presented in Fig. 3. Taking Eq. (19) into account, Fig. 3 can be simplified to Fig. 4.

In order to extract B, two steady speeds with time interval τ (t and $t+\tau$) are required, as is shown in Fig. 5a, where the acceleration of the velocity is 0 at t_0 and $t_0+\tau$, two disturbance estimates can be obtained according to Eq. (6) as

$$\hat{d}(t_0) = -\Delta\hat{J}\dot{\omega}(t_0) - \Delta\hat{B}\omega(t_0) - T_L \tag{20}$$

$$\hat{d}(t_0+\tau) = -\Delta\hat{J}\dot{\omega}(t_0+\tau) - \Delta\hat{B}\omega(t_0+\tau) - T_L \tag{21}$$

The subtraction of Eqs. (20) and (21) gives

$$\Delta\hat{B} = -\frac{\hat{d}(t_0+\tau) - \hat{d}(t_0)}{\omega(t_0+\tau) - \omega(t_0)} \tag{22}$$
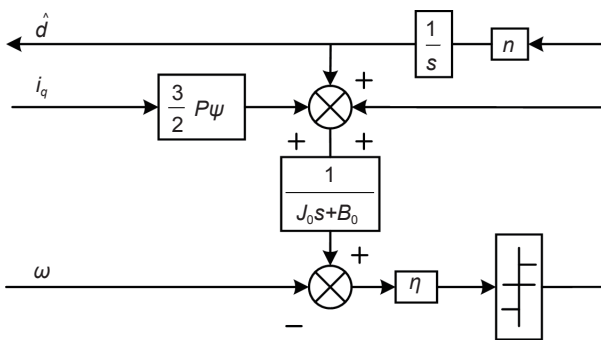
Then, the estimated value of $\hat{B}$ is described as

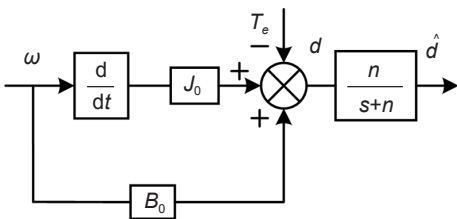**Fig. 3   Structural block diagram of ESMO.**

Fig. 4   Equivalent LPF structural block diagram.
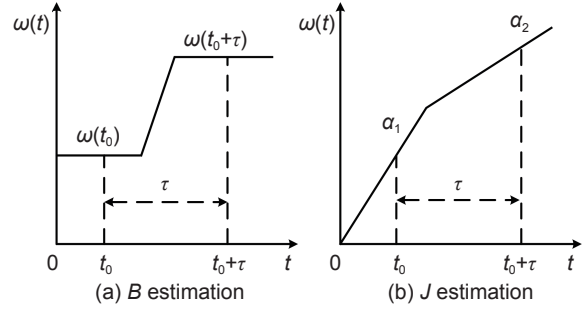

Fig. 5   Process of parameter identification.

$$\hat{B} = B_0 + \Delta\hat{B} = B_0 - \frac{\hat{d}(t_0+\tau) - \hat{d}(t_0)}{\omega(t_0+\tau) - \omega(t_0)} \tag{23}$$

After obtaining $\hat{B}$ and updating the value of B_0 in Eq. (7), the disturbance estimate is rewritten as

$$\hat{d} = -\Delta\hat{J}\dot{\omega} - T_L \tag{24}$$

When the motor is operated at two accelerations (α_1 and α_2) with time interval τ (t and $t+\tau$), as shown in Fig. 5b, the two disturbance estimates can be obtained according to Eq. (24) as

$$\hat{d}(t_0) = -\Delta\hat{J} \cdot \alpha_1 - T_L \tag{25}$$

$$\hat{d}(t_0+\tau) = -\Delta\hat{J} \cdot \alpha_2 - T_L \tag{26}$$

The subtraction of Eqs. (25) and (26) gives

$$\Delta\hat{J} = -\frac{\hat{d}(t_0+\tau) - \hat{d}(t_0)}{\alpha_2 - \alpha_1} \tag{27}$$

The estimated value of $\hat{J}$ is described as

$$\hat{J} = J_0 + \Delta\hat{J} = J_0 - \frac{\hat{d}(t_0+\tau) - \hat{d}(t_0)}{\alpha_2 - \alpha_1} \tag{28}$$

After the estimated values of B and J have been obtained, the value of the load torque can be derived directly according to Eq. (4), but the accuracy of load torque will completely depend on the accuracy of the above two values. As a result, the load torque is identified separately aiming at minimizing the impact of coupling between the parameters and ensuring the reliability of the parameter identification results.

2.2   Load torque identification based on Luenberger observer

The load torque is identified by using a state observer since the load torque cannot be obtained by direct measurement and the state observer is simple in structure and has a strong real-time capability, but the conventional open-loop state observer does not have an output feedback correction link, and the accuracy and convergence speed of the final identification results will have some errors with the expected value[32, 33]. Therefore, the Luenberger observer is designed for the

identification of load torque.

In a linear constant system $\sum_0 (A, B, C)$:

$$\begin{cases} \dot{x} = Ax + Bu, \\ y = Cx \end{cases} \tag{29}$$

where x, u, and y denote the system's state variable, input, and output, respectively; and A, B, and C represent the system matrix, input matrix, and output matrix, respectively. Refactor the system to get

$$\begin{cases} \dot{\hat{x}} = A\hat{x} + Bu, \\ \hat{y} = C\hat{x} \end{cases} \tag{30}$$

where $\hat{x}$ and $\hat{y}$ represent two estimated values of the state variable and system output, respectively.

As for observation systems, when the observed state $\hat{x}$ is inconsistent with the practical value x, its output $\hat{y}$ is also inconsistent with the practical value y, ultimately an output error signal $y - \hat{y}$ will be generated. If the signal is feedback to the front of the integrator to correct $\hat{x}$, $\hat{x}$ can be asymptotically approximated to actual value x. The output feedback error matrix G is introduced to correct the errors by feedback. To summarize, a closed-loop Luenberger observer with feedback error analysis is established as indicated in Eq. (31).

$$\begin{cases} \dot{\hat{x}} = A\hat{x} + Bu + G(y - \hat{y}), \\ \hat{y} = C\hat{x} \end{cases} \tag{31}$$

Bringing the output equation into the state equation, the Luenberger observer becomes

$$\begin{cases} \dot{\hat{x}} = (A - GC)\hat{x} + Bu + Gy, \\ \hat{y} = C\hat{x} \end{cases} \tag{32}$$

According to Eq. (5), when electromagnetic torque T_e is defined as the input, mechanical angular velocity ω and load torque T_L are defined as the state variables, and the mechanical angular velocity ω is defined as the system output, the observed objects are ω and T_L. Assuming that the load torque remains constant during the measurement time, the state space expression of the observed system is listed according to Eq. (29) as

$$\begin{bmatrix} \dot{\omega} \\ \dot{T}_L \end{bmatrix} = A \begin{bmatrix} \omega \\ T_L \end{bmatrix} + BT_e, \begin{bmatrix} \omega \\ 0 \end{bmatrix} = C \begin{bmatrix} \omega \\ T_L \end{bmatrix} \tag{33}$$

where $A = \begin{bmatrix} -BJ^{-1} & -J^{-1} \\ 0 & 0 \end{bmatrix}$, $B = \begin{bmatrix} J^{-1} & 0 \end{bmatrix}^{\mathrm{T}}$, $C = \begin{bmatrix} 1 & 0 \end{bmatrix}$.

For a state observation system, the necessary and sufficient condition for the existence of the observer is that the system must be completely observable, or its non-observable subsystems are asymptotically stable. The observable system's observability matrix N is constructed as

$$N = \begin{bmatrix} C \\ CA \end{bmatrix} = \begin{bmatrix} 1 & 0 \\ -BJ^{-1} & -J^{-1} \end{bmatrix} \tag{34}$$

It is clear that the system has a full rank of 2 for N. Therefore, the constructed observed system is fully observable. According to Eq. (33), the Luenberger load torque observer is obtained according to design principle as

$$\begin{cases} \begin{bmatrix} \dot{\hat{\omega}} \\ \dot{\hat{T}}_L \end{bmatrix} = A \begin{bmatrix} \hat{\omega} \\ \hat{T}_L \end{bmatrix} + BT_e + G(\omega - \hat{\omega}), \\ \hat{\omega} = C \begin{bmatrix} \hat{\omega} \\ \hat{T}_L \end{bmatrix} \end{cases} \tag{35}$$

where $\hat{T}_L$ is the observed values of load torque and G is the feedback matrix and $G = [g_1 \ g_2]^{\mathrm{T}}$, where g_1 and g_2 are constants.

According to Eq. (35), Fig. 6 depicts a block schematic of the construction of the Luenberger load torque observer. For applicability to numerical calculation systems, the above load torque observer is discretized by Euler method and described as

$$\begin{cases} \hat{\omega}(k) = \hat{\omega}(k-1) + T_s[J^{-1}\left(T_e(k-1) - \hat{T}_L(k-1)\right) + \\ \qquad g_1\tilde{\omega}(k-1) - BJ^{-1}\tilde{\omega}(k-1)], \\ \hat{T}_L(k) = \hat{T}_L(k-1) + T_s g_2 \tilde{\omega}(k-1) \end{cases} \tag{36}$$

where T_s is the sampling time, and $\tilde{\omega}(k-1) = \omega(k-1) - \hat{\omega}(k-1)$ is the observed mechanical angular velocity error with time at $k-1$.

Subtracting Eq. (36) from Eq. (33) gives the state error equation as

$$\begin{bmatrix} \dot{\tilde{\omega}} \\ \dot{\tilde{T}}_L \end{bmatrix} = (A - GC) \begin{bmatrix} \tilde{\omega} \\ \tilde{T}_L \end{bmatrix} = \begin{bmatrix} -BJ^{-1} - g_1 & -J^{-1} \\ -g_2 & 0 \end{bmatrix} \begin{bmatrix} \tilde{\omega} \\ \tilde{T}_L \end{bmatrix} \tag{37}$$

where $\tilde{\omega}$ and $\tilde{T}_L$ are the observation errors for the angular velocity and load torque, respectively. For the observer's convergence, it should be ensured that $A - GC$ has a negative real part, as can be seen from Eq. (38):

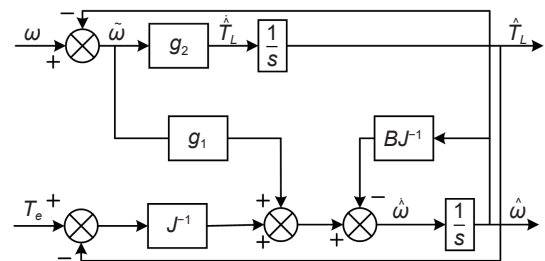$$(A - GC) = \begin{bmatrix} -BJ^{-1} - g_1 & -J^{-1} \\ -g_2 & 0 \end{bmatrix} \tag{38}$$

Fig. 6   Structure of the Luenberger load torque observer.

Establishing the characteristic equation and organizing it give

$$s^2 + \left(BJ^{-1} + g_1\right)s - g_2 J^{-1} = 0 \qquad (39)$$

To simplify the problem, we assume that there are two equal negative roots, r_1 and r_2 ($r_1 = r_2 < 0$), which are brought into Eq. (39), and we can get

$$s^2 - 2r_1 s + r_1^2 = 0 \qquad (40)$$

Comparing the coefficients of Eqs. (39) and (40), we can get

$$\begin{cases} g_1 = -2r_1 - BJ^{-1}, \\ g_2 = -Jr_1^2 \end{cases} \qquad (41)$$

From Eq. (41), BJ^{-1} is small enough to be ignored, and it can be seen that as long as $g_1 > 0$ and $g_2 < 0$, the characteristic roots of $A - GC$ are guaranteed to locate in the left half plane of the complex frequency domain, indicating that the state observer's output will eventually converge to the actual state variables. Due to the fact that the values of g_1 and g_2 affect the stability and response speed of the system, it also can be seen from Eq. (41) that B and J do not affect the convergence of the load torque observation, but only the speed of convergence.

Besides, considering whether the two observers will affect each other and thus affect the whole parameter identification result, we conducted the following analysis.

Firstly, it can be seen from the overall structure diagram of the observer shown in Fig. 2 that the two observers establish the state equations according to i_q and ω of the PMSM, and extract the required parameters information from them. Therefore, the two observers are independent of each other in the source of information acquisition. Secondly, as we have discussed in Section 2.1, the effectiveness of ESMO's parameter identification is only related to the choice of η and n, which affect the stability and convergence speed of the observer, respectively. Thirdly, as we discussed before, the identification effect of Luenberger observer is influenced by g_1, g_2, B, and J, while B and J only affect the rate of convergence. As a result, the identification of the parameters by the two observers is carried out independently, and the identification results of T_L are not affected by B and J, which is also the embodiment of the decoupling of the parameter identification. In consequence, the stability analysis of the two observers is carried out separately, in this case the required parameters can be decoupled.

3 Adaptive Gains Adjustment and Disturbance Compensation

When the system parameters are static or vary slightly in the PMSM double closed-loop control system, the controller gains adjusted according to the traditional approach or work experience can artificially acquire good enough performance. However, the parameters of the controller will inevitably vary throughout system operation, and if the controller gains cannot be modified effectively in time, the control performance of the system may be affected and instability may occur. As a result, it is critical to develop a method for fulfilling the controller gains self-tuning to heighten the robustness and anti-interference capability of the controller so that it is suitable for a wide range of operating situations. Choosing the third-order best design method[34] to correct the controller in series for the PI controller may give the transfer function the highest phase angle margin and make the stability and dynamics of the system reach the optimum condition. The current loop in the PMSM control system has a significantly smaller time constant than the speed loop, where the current loop can be simplified and regarded as a component of the speed loop. Therefor the entire system is equivalent to a second-order system with a zero point. Figure 7 shows a simplified comparable block diagram, where ω^* is the motor's provided speed, K_p is the speed loop's proportionality coefficient, K_i is the speed loop's integration coefficient, $T_i = L/R_s$ is the current loop's closed loop time constant, and $K_\tau = 1.5P^2\psi$ is the motor's torque coefficient. Figure 7 shows the open-loop transfer function as

$$G(s) = \frac{K_\tau \left(K_p s + K_i\right)}{s(Js + B)(T_i s + 1)} \qquad (42)$$

Let $K = \dfrac{K_\tau K_i}{B}$, $T_1 = \dfrac{K_p}{K_i}$, and $T_2 = \dfrac{J}{B}$, then Eq. (42) becomes

$$G(s) = \frac{K(T_1 s + 1)}{s(T_2 s + 1)(T_i s + 1)} \qquad (43)$$

According to the third-order optimal method, the series correction of Eq. (43) is carried out. We design the correction function as $G_i(s) = (T_i s + 1)/s$. Since $T_2 \gg T_i$, the corrected transfer function is obtained as
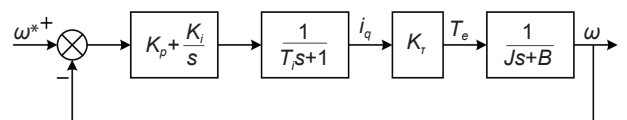

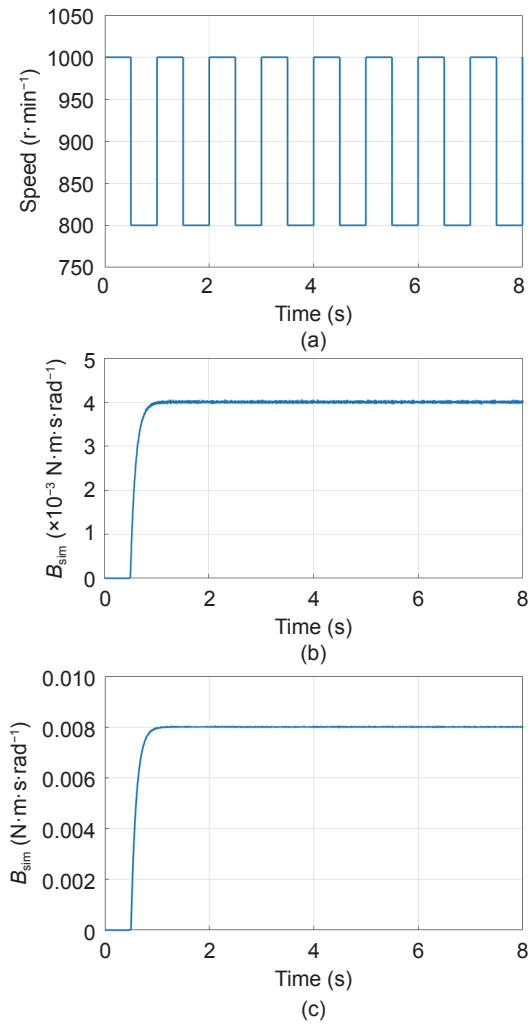**Fig. 7　Simplified equivalent speed-loop block diagram.**

$$G'(s) = \frac{K(T_1 s + 1)}{s^2 (T_2 s + 1)} \tag{44}$$

The design parameter selection equations are $h = \dfrac{T_1}{T_2} = 5$ and $K = \dfrac{1}{8T_2^2}$. Thus, the parameters of the PI regulator are obtained as

$$K_p = \frac{hJ}{8T_2 K_\tau} \tag{45}$$

$$K_i = \frac{B}{8T_2^2 K_\tau} \tag{46}$$

where h is the intermediate frequency bandwidth of the open-loop Bode plot of the corrected transfer function.

The speed loop's adaptive gain value may be obtained through plugging identified values of B and J into Eqs. (45) and (46), and then the PI parameter self-tuning function of the PMSM control system can be accomplished.

Considering the current loop's tracking speed is significantly faster than that of the speed loop, when the load torque changes, the speed loop will take longer to respond, resulting in a higher influence on the motor speed. The load torque observed by the Luenberger observer is feedforward compensated to the current loop of the motor based on the rapidity of the current loop response, so that the disturbance acts directly on the given current, where the feedforward effect is introduced to the feedback system without impacting its stability, and the system becomes more responsive to disturbances. When the load changes suddenly, it will directly lead to the change of the given current, thus leading to the change of the error current. The error current passes through the circuit PI regulator and causes the output to change, allowing the motor to immediately adjust the output torque and balance the load disturbance quickly, so that the speed will be less affected.

According to the speed loop control block diagram shown in Fig. 8, it is considered that the response of the current loop is fast enough to ignore the time delay of the current loop. Feedforward compensation is implemented according to load torque.

In Fig. 8, K_c is the load torque compensation factor. According to the full compensation condition for feedforward compensation, we can get

$$K_c = \frac{2}{3P\psi} \tag{47}$$

Figure 9 shows the system's final vector control block diagram.

4   Simulation Verification

4.1   Parameter identification verification

In this part, simulations are conducted by employing MATLAB/Simulink with the parameters listed in Table 1 to evaluate the reliability of proffered methods. Besides, the relevant parameters are designed as follows: $\eta = -2$, $n = 100$, $\tau = 0.5$ s, $g_1 = 6$, $g_2 = -0.0043$, and assuming $B_0 = 0$ N·m·s·rad^{-1}, $J_0 = 0$ kg·m^2. Due to the different identification conditions for B and J, the two parameters are identified individually.

In the identification of B, a rectangular varying

Fig. 8   Block diagram of speed loop control with feedforward compensation.

Fig. 9   System's vector control block diagram.

Table 1   PMSM parameters specification.

Parameter	Value
Inductance	$L_d = L_q = 0.009$ H
Number of pole pairs	$P = 4$
Moment of inertia	$J = 0.003$ kg·m²
Flux linkage	$\psi = 0.175$ Wb
Stator resistance	$R = 2.6\ \Omega$
Viscous friction coefficient	$B = 0.004$ N·m·s·rad⁻¹

speed is given, as shown in Fig. 10a. Experiments were conducted with $B =0.004$ N·m·s·rad⁻¹ and $B= 0.008$ N·m·s·rad⁻¹, respectively. Figures 10b and 10c depict the simulation results, and B_{sim} represents the value of simulation result.

The simulation results reveal that after a brief delay, all of the estimation curves converge to the set value of 4 N·m·s·rad⁻¹ or 8 N·m·s·rad⁻¹, demonstrating that the suggested approach is capable of properly estimating

parameter B.

Furthermore, the identification of J needs to be carried out at a variable speed, given a sawtooth wave-like variation speed, as shown in Fig. 11a, to validate the identification effect at $J=0.003$ kg·m² and $J= 0.009$ kg·m², respectively. Simulation results are revealed in Figs. 11b and 11c, and J_{sim} represents the value of simulation result.

As demonstrated by the simulation outcomes, after a short delay all the estimation curves converge to the system configuration of 0.003 kg·m² or 0.009 kg·m², proving the proposed method is capable of properly estimating the parameter J.

Moreover, the load torque was determined in two situations as the given load increase suddenly from 2 N·m to 4 N·m and decrease suddenly from 4 N·m to 2 N·m at 2 s, and Fig. 12 illustrates the outcomes of the

Fig. 10 Viscous friction identification results. (a) Rectangular varying speed. (b) $B =0.004$ N·m·s·rad⁻¹ simulation result. (c) $B=0.008$ N·m·s·rad⁻¹ simulation result.
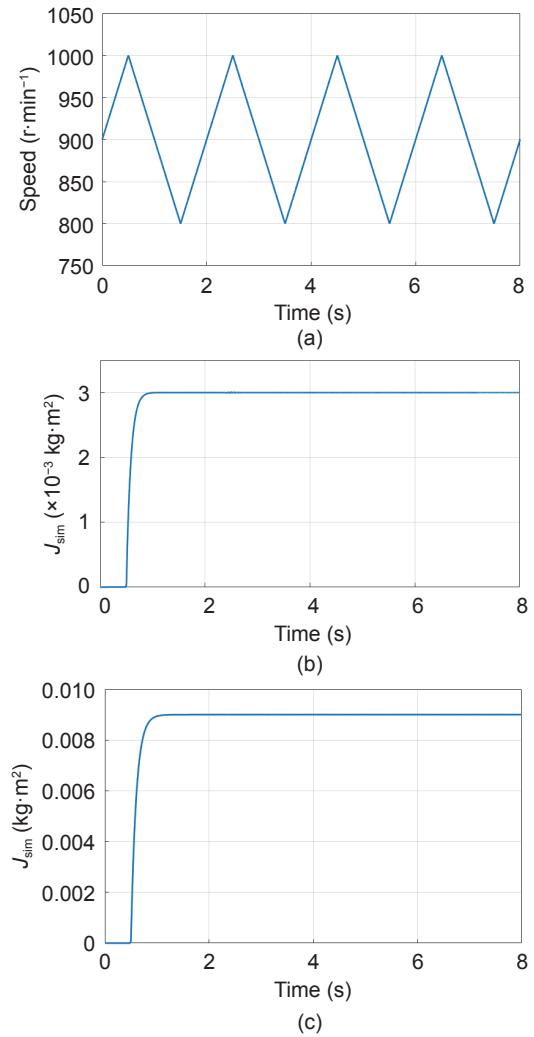
Fig. 11 Moment of inertia identification results. (a) Sawtooth wave-like varying speed. (b) $J =0.003$ kg·m² simulation result. (c) $J=0.009$ kg·m² simulation result.
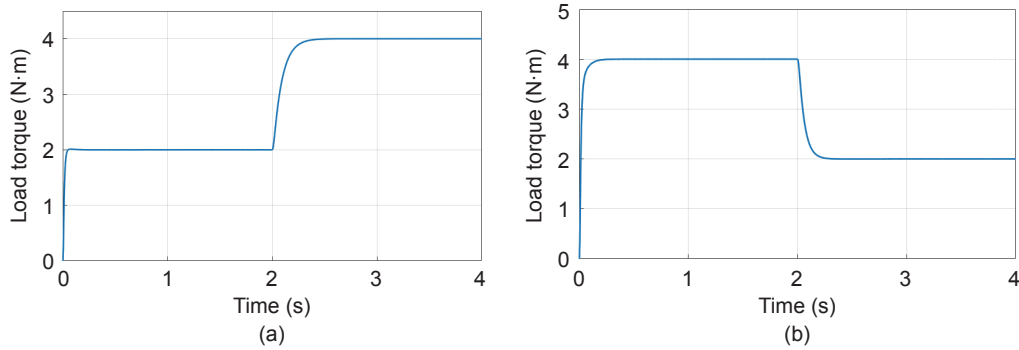
Fig. 12   Load torque identification results. (a) Identification results of load surging from 2 N·m to 4 N·m. (b) Identification results of load dropping from 4 N·m 2 N·m.

identification process.

From the experimental outcomes, it can be seen that the proposed parameter identification method has strong dynamic tracking capabilities and high precision.

In addition, to verify the effect of noise on the ESMO observer, we added electrical torque noise to disturbance signal d. According to Eq. (6), we can get

$$d' = -\Delta J\dot{\omega} - \Delta B\omega - T_L + T_e' \qquad (48)$$

At this point with a given speed as shown in Fig. 13, we added noise T_e' to T_e and the result is shown in Fig. 14.

After the noise was added, the disturbance information d' before and after being filtered by ESMO's equivalent LPF are shown in Fig. 15. It can be seen that the equivalent LPF of ESMO has a good
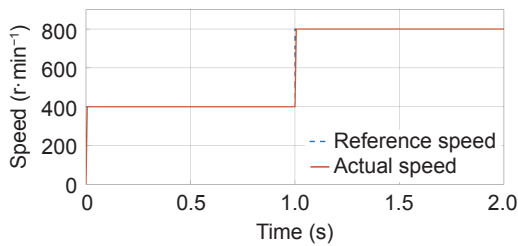
Fig. 13   Waveform of the given speed changing from 400 r·min⁻¹ to 800 r·min⁻¹.
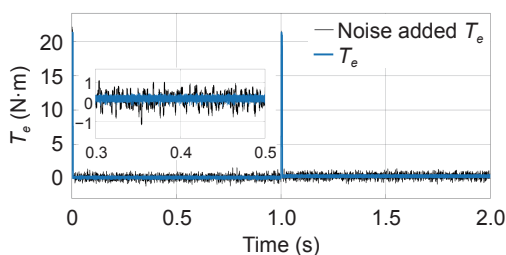
Fig. 14   Waveform of T_e before and after noise being added.
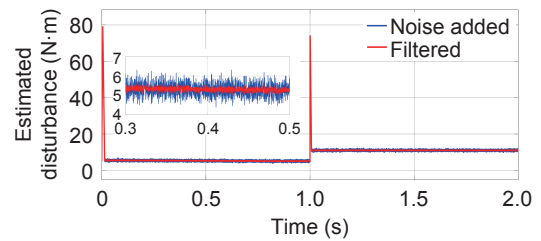
Fig. 15   Waveform of estimated disturbance before and after being filtered.

filtering effect.

4.2   Verification of the effect of self-tuning and loads compensation

A speed that fluctuates in a sawtooth waveform is presented to validate the self-tuning effect of the proposed approach, and a load is added at 2 s to compare the speed control effect with conventional PI control.

Firstly, the experimental outcomes were compared in pairs utilizing the control variable approach in three cases to get a sharper contrast effect.

When B is constant, the speed waveforms at $J=$ 0.003 kg·m² and $J =$0.009 kg·m² are depicted in Figs. 16a and 16b. When J changes, it can be noticed that the speed after self-tuning has a faster convergence speed and a reduced overshoot when compared to conventional PI control.

When J is constant, the speed waveforms at $B=$ 0.004 N·m·s·rad⁻¹ and $B =$0.008 N·m·s·rad⁻¹ are depicted in Figs. 16b and 16c. It can be observed that when B changes, the speed self-tuned can still converge quickly, as well as the loads compensation condition. In comparison, although the speed waveform under conventional PI control method possesses a quicker responding speed, an obvious overshoot exists still, and the speed cannot eventually converge to the regulated speed.
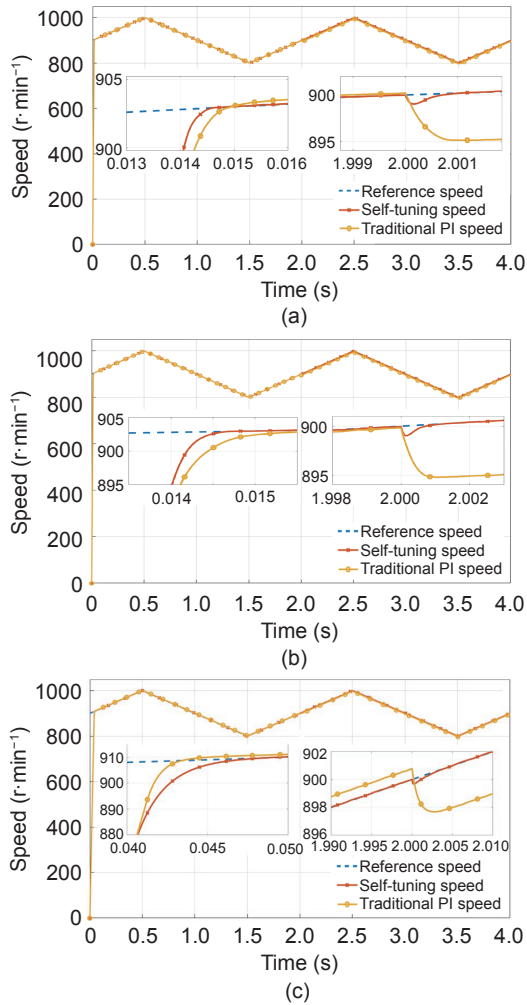
Fig. 16 Speed waveforms. (a) *B* =0.004 N·m·s·rad⁻¹, *J*= 0.003 kg·m². (b) *B* =0.004 N·m·s·rad⁻¹, *J* =0.009 kg·m². (c) *B*=0.008 N·m·s·rad⁻¹, *J*=0.009 kg·m².

The results show that the adaptive gain adjustment and disturbance compensation method based on parameter identification proposed in this paper has good robustness, effectiveness, and reliability.

Secondly, in order to verify the effectiveness of the proposed Luenberger observer in compensating for load disturbances, experiment combining traditional PI control with the Luenberger observer was carried out. There were three sets of control methods established to obtain a clearer comparison effects. They were the aforementioned adaptive control method, the traditional PI method, and the combination of traditional PI and the Luenberger observer.

When *B* =0.004   N·m·s·rad⁻¹, *J* =0.003   kg·m², assuming that the motor parameters are nameplate values, it can be seen from Fig. 17a that the speed has a faster convergence rate after the adaptive PI parameter adjustment during the speed rise period. After
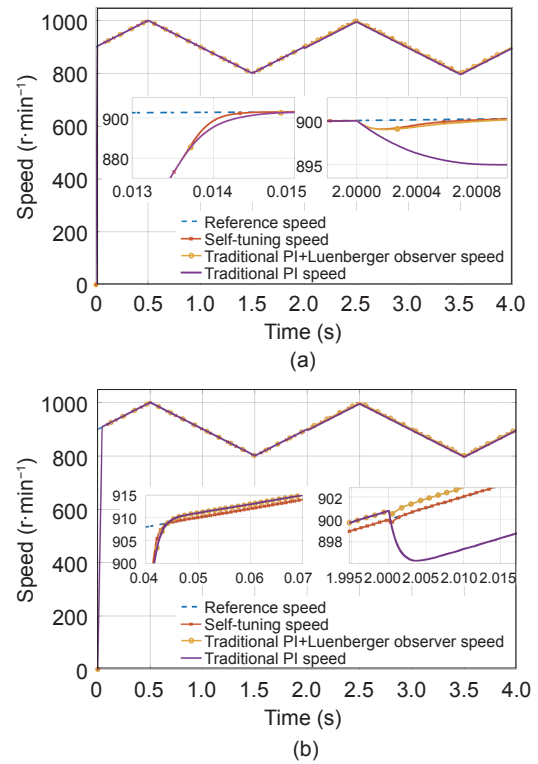
Fig. 17 Adaptive control effects of the combination of traditional PI and Luenberger observer. (a) *B*= 0.004 N·m·s·rad⁻¹, *J*=0.003 kg·m². (b) *B*=0.004 N·m·s·rad⁻¹, *J*=0.009 kg·m².

encountering a load disturbance at 2 s, the speed can converge to the given value after compensation based on the load torque observed by the Luenberger observer. In contrary, there is a large deviation in speed under traditional PI control as a consequence of no disturbance compensation.

When the parameter is changed (*J* varies from 0.003 to 0.009 kg·m²), it can be seen from Fig. 17b that the speed self-tuned can still converge quickly, as well as the loads compensation condition. On the other hand, method combining traditional PI control with the Luenberger observer is still able to accurately identify and compensate for disturbances to some extent, although the speed has already overshot. At this moment, compared with traditional PI control, the speed compensated based on the load torque observed by the Luenberger observer is much less affected by load disturbance in some extent.

The above analysis indicates that the Luenberger observer is able to identify load torque independent of ESMO and can compensate for it accurately.

Thirdly, in order to further verify the effect of designing the Luenberger observer alone on the decoupling of parameter identification results,

experiments to identify T_L by ESMO and the Luenberger observer were conducted separately.

From the discussion in Section 2.1, it is clear that after the estimated values of B and J have been obtained, the value of the load torque can be derived directly according to Eq. (4).

Suppose that the effect of self-tuning of ESMO fails due to some uncontrollable factor (e.g., mechanical ageing). Under this condition, substituting the values of T_e and ω of the motor into Eq. (4), when J varied from 0.003 to 0.009 kg·m^2, the results of the speed control effect at T_L identified by ESMO and the Luenberger observer are shown in Fig. 18 in red and green separately.

It can be seen from Fig. 18 that when the parameters were changed, the speed is slightly overshot by the PI control which loses its self-tuning effect. When a disturbance is encountered, the ESMO-identified T_L has a large error with the given value after compensation, while the Luenberger observer-identified T_L still has a slight error but can significantly reduce the effect of the disturbance after compensation, showing that designing the Luenberger observer alone possesses a positive impact on the decoupling of parameter identification results.

5 Conclusion

This paper proposed a mechanical parameter identification approach based on an integrated observer framework and the identification results are employed for adaptive control and disturbance compensation in a PMSM vector control system. In the parameter identification part, the viscous friction coefficient and the moment of inertia are identified by ESMO, where the equivalent LPF may avoid the chattering, phase lag, and amplitude decay generated by the additional LPF, and the cutoff frequency of the equivalent LPF can be
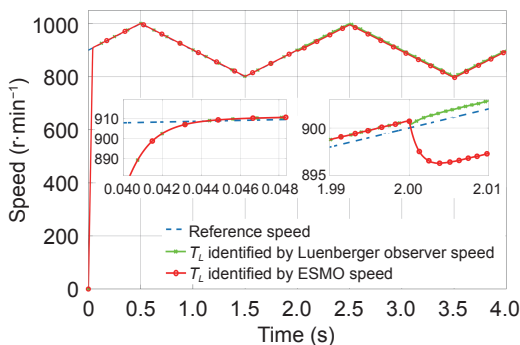
Fig. 18 Waveform of speed for T_L identified by Luenberger observer and ESMO.

customized as required. Then, by designing a separate Luenberger observer for load torque identification, the influence of parameter coupling may be reduced, and high precision and real-time performance can be achieved.

Acknowledgment

References

[1] S. Fang, H. Liu, H. Wang, H. Yang, and H. Lin, High power density PMSM with lightweight structure and high-performance soft magnetic alloy core, *IEEE Trans. Appl. Superconduct.*, vol. 29, no. 2, pp. 1–5, 2019.

[2] T. Türker, U. Buyukkeles, and A. F. Bakan, A robust predictive current controller for PMSM drives, *IEEE Trans. Ind. Electron.*, vol. 63, no. 6, pp. 3906–3914, 2016.

[3] Y. Zhao and L. Dong, Robust current and speed control of a permanent magnet synchronous motor using SMC and ADRC, (in Chinese), *Control Theory and Technology*, vol. 17, no. 2, pp. 190–199, 2019.

[4] Y. Shen, L. Yu, and J. Li, Robust electric vehicle routing problem with time windows under demand uncertainty and weight-related energy consumption, *Complex System Modeling and Simulation*, vol. 2, no. 1, pp. 18–34, 2022.

[5] K. -H. Kim and M. -J. Youn, A nonlinear speed control for a PM synchronous motor using a simple disturbance estimation technique, *IEEE Trans. Ind. Electron.*, vol. 49, no. 3, pp. 524–535, 2002.

[6] C. Lian, F. Xiao, S. Gao, and J. Liu, Load torque and moment of inertia identification for permanent magnet synchronous motor drives based on sliding mode observer, *IEEE Trans. Power Electron.*, vol. 34, no. 6, pp. 5675–5683, 2019.

[7] M. S. Carmeli, F. Castelli-Dezza, M. Iacchetti, and R. Perini, Effects of mismatched parameters in MRAS sensorless doubly fed induction machine drives, *IEEE Trans. Power Electron.*, vol. 25, no. 11, pp. 2842–2851, 2010.

[8] A. M. El-Garhy and M. E. El-Shimy, BELBIC for MRAS with highly non-linear process, *Alex. Eng. J.*, vol. 54, no. 1, pp. 7–16, 2015.

[9] I. Benlaloui, S. Drid, L. Chrifi-Alaoui, and M. Ouriagli, Implementation of a new MRAS speed sensorless vector control of induction machine, *IEEE Trans. Energy*

Conversion, vol. 30, no. 2, pp. 588–595, 2015.

[10] H. M. Kojabadi and M. Ghribi, MRAS-based adaptive speed estimator in PMSM drives, in *Proc. 9th IEEE International Workshop on Advanced Motion Control*, Istanbul, Turkey, 2006, pp. 569–572.

[11] S. J. Underwood and I. Husain, Online parameter estimation and adaptive control of permanent-magnet synchronous machines, *IEEE Trans. Ind. Electron.*, vol. 57, no. 7, pp. 2435–2443, 2010.

[12] Y. Yu, X. Huang, Z. Li, M. Wu, T. Shi, Y. Cao, G. Yang, and F. Niu, Full parameter estimation for permanent magnet synchronous motors, *IEEE Trans. Ind. Electron.*, vol. 69, no. 5, pp. 4376–4386, 2022.

[13] F. Tinazzi, P. G. Carlet, S. Bolognani, and M. Zigliotto, Motor parameter-free predictive current control of synchronous motors by recursive least-square self-commissioning model, *IEEE Trans. Ind. Electron.*, vol. 67, no. 11, pp. 9093–9100, 2020.

[14] A. Brosch, S. Hanke, O. Wallscheid, and J. Böcker, Data-driven recursive least squares estimation for model predictive current control of permanent magnet synchronous motors, *IEEE Trans. Power Electron.*, vol. 36, no. 2, pp. 2179–2190, 2021.

[15] M. Messaoudi, H. Kraiem, M. B. Hamed, L. Sbita, and M. N. Abdelkrim, A robust sensorless direct torque control of induction motor based on MRAS and extended Kalman filter, *Leonardo J. Sci.*, vol. 12, no. 1, pp. 35–56, 2008.

[16] T. Boileau, N. Leboeuf, B. Nahid-Mobarakeh, and F. Meibody-Tabar, Online identification of PMSM parameters: Parameter identifiability and estimator comparative study, *IEEE Trans. Ind. Applicat.*, vol. 47, no. 4, pp. 1944–1957, 2011.

[17] X. Jiang, P. Sun, and Z. Q. Zhu, Modeling and simulation of parameter identification for PMSM based on EKF, in *Proc. 2010 Int. Cof. Computer, Mechatronics, Control and Electronic Engineering*, Changchun, China, 2010, pp. 345–348.

[18] T. Boileau, B. Nahid-Mobarakeh, and F. Meibody-Tabar, On-line identification of PMSM parameters: Model-reference vs EKF, in *Proc. 2008 IEEE Ind. Applicat. Soc. Annu. Meeting*, Edmonton, Canada, 2008, pp. 1–8.

[19] A. Avdeev and O. Osipov, PMSM identification using genetic algorithm, in *Proc. 2019 26th Int. Workshop on Electric Drives: Improvement in Efficiency of Electric Drives (IWED)*, Moscow, Russia, 2019, pp. 1–4.

[20] W. Gong, Z. Liao, X. Mi, L. Wang, and Y. Guo, Nonlinear equations solving with intelligent optimization algorithms: A Survey, *Complex System Modeling and Simulation*, vol. 1, no. 1, pp. 15–32, 2021.

[21] Y. Tang, L. Li, and X. Liu, State-of-the-art development of complex systems and their simulation methods, *Complex System Modeling and Simulation*, vol. 1, no. 4, pp. 271–290, 2021.

[22] Y. Shen, D. Wu, and Z. Ji, Model reference fuzzy adaptive control of permanent magnet synchronous motor, in *Proc.*

2006 Chinese Control Conference, Harbin, China, 2006, pp. 1522–1527.

[23] S. Wang, G. Yang, Z. Qu, S. Shi, and C. Chen, Identification of PMSM based on EKF and elman neural network, in *Proc. 2009 IEEE International Conference on Automation and Logistics*, Shenyang, China, 2009, pp. 1459–1463.

[24] W. Xu, Y. Jiang, and C. Mu, Novel composite sliding mode control for PMSM drive system based on disturbance observer, *IEEE Trans. Appl. Superconduct.*, vol. 26, no. 7, p. 0612905, 2016.

[25] S. Ye and X. Yao, An enhanced SMO-based permanent-magnet synchronous machine sensorless drive scheme with current measurement error compensation, *IEEE J. Emerging Select. Topics Power Electronics*, vol. 9, no. 4, pp. 4407–4419, 2020.

[26] K. Liu, J. Feng, S. Guo, L. Xiao, and Z. -Q. Zhu, Identification of flux linkage map of permanent magnet synchronous machines under uncertain circuit resistance and inverter nonlinearity, *IEEE Trans Ind. Informat.*, vol. 14, no. 2, pp. 556–568, 2018.

[27] W. Lu, B. Tang, K. Ji, K. Lu, D. Wang, and Z. Yu, A new load adaptive identification method based on an improved sliding mode observer for PMSM position servo system, *IEEE Trans. Power Electron.*, vol. 36, no. 3, pp. 3211–3223, 2020.

[28] B. Wang, Y. Shao, Y. Yu, Q. Dong, Z. Yun, and D. Xu, High-order terminal sliding-mode observer for chattering suppression and finite-time convergence in sensorless SPMSM drives, *IEEE Trans. Power Electron.*, vol. 36, no. 10, pp. 11910–11920, 2021.

[29] L. Yi, C. Zhang, and G. Wang, Research of self-tuning PID for PMSM vector control based on improved KMTOA, *International Journal of Intelligent Systems and Applications*, vol. 9, no. 3, pp. 60–67, 2017.

[30] D. Xu and Y. Gao, A simple and robust speed control scheme of permanent magnet synchronous motor, (in Chinese), *Control Theory and Applications*, vol. 2, no. 2, pp. 165–168, 2004.

[31] W. Gao and Z. P. Jiang, Learning-based adaptive optimal output regulation of linear and nonlinear systems: An overview, (in Chinese), *Control Theory and Technology*, no. 1, pp. 1–19, 2022.

[32] A. Accetta, M. Cirrincione, M. Pucci, and G. Vitale, Neural sensorless control of linear induction motors by a full-order Luenberger observer considering the end effects, *IEEE Trans. Ind. Applicat.*, vol. 50, no. 3, pp. 1891–1904, 2013.

[33] L. He, F. Wang, J. Wang, and J. Rodríguez, Zynq implemented luenberger disturbance observer based predictive control scheme for PMSM drives, *IEEE Trans. Power Electron.*, vol. 35, no. 2, pp. 1770–1778, 2019.

[34] J. Yu, Design of series corrector based on the third-order best design, (in Chinese), *Industrial Instrumentation and Automation*, no. 6, pp. 109–116, 2013.

Zhong Liao received the BEng degree in electrical engineering and automation from Southwest Jiaotong University, China, in 2019. He is currently pursuing the MS degree in electrical engineering at Hunan University of Science and Technology, Xiangtan, China. His current research interests include parameter identification and adaptive control for permanent magnet synchronous motor.

Zhaohua Liu received the MSc degree in computer science and engineering, and the PhD degree in automatic control and electrical engineering from Hunan University, China in 2010 and 2012, respectively. He worked as a visiting researcher in the Department of Automatic Control and Systems Engineering at University of Sheffield, United Kingdom from 2015 to 2016. He is currently a professor of automatic control and systems with the School of Information and Electrical Engineering, Hunan University of Science and Technology, Xiangtan, China. His current research interests include intelligent information processing and control of wind turbines, computational intelligence and learning algorithms design, machine learning aided fault diagnosis and prognosis, parameter estimation and intelligent control of permanent-magnet synchronous machine drives, and fault diagnosis based intelligent operations and maintenance for electric power equipment. He is a regular reviewer for several international journals and conferences. He has published more than 50 research papers in refereed journals and conferences, including IEEE Transactions/journal/magazine. He is a regular reviewer for several international journals and conferences.

Mingyang Lyu received the PhD degree in control theory and engineering from Hunan University, China in 2020. He is currently a lecturer with the School of Information and Electrical Engineering, Hunan University of Science and Technology, Xiangtan, China. His research interests include chaos theory and application, and modeling for complex process industries based on machine learning and deep learning.

Dian Wang is currently a professor level senior engineer of CRRC Zhuzhou Institute Co., Ltd. He is mainly engaged in the design of complete machine systems, wind turbine dynamics control and fault diagnosis, etc.

Lei Chen received the MS degree in computer science and engineering, and the PhD degree in automatic control and electrical engineering from Hunan University, China in 2012 and 2017, respectively. He is currently a lecturer with the School of Information and Electrical Engineering, Hunan University of Science and Technology, Xiangtan, China. His current research interests include deep learning, network representation learning, information security of industrial control system, and industrial big data analysis.

Faming Wu received the PhD degree in mechanical engineering from Lanzhou University of Technology in 2021. He is currently a professor level senior engineer of CRRC Zhuzhou Institute Co., Ltd. He is mainly engaged in wind power technology and equipment.

Zhengheng Wang received the BSc and MSc degrees in automation from Beijing University of Chemical Technology (BUCT), China, and the PhD degree in natural resource engineering from Laurentian University (LU), Canada. He is currently serving as a lecturer in Hunan University of Science and Technology (HNUST). His primary research interest includes intelligent control, process fault diagnosis, and artificial intelligence related subjects.

Hualiang Wei received the PhD degree in automatic control from University of Sheffield, Sheffield, UK, in 2004. He is currently a senior lecturer with the Department of Automatic Control and Systems Engineering, University of Sheffield, Sheffield, UK. His research focuses on identification and modelling for complex nonlinear systems, model and parameter estimation, signal processing, feature engineering, pattern recognition and classification, and interpretable machine learning, among others.